

New iodine-apatites: synthesis and crystal structure

Evgeny N. BULANOV* , Sergey S. PETROV , Alexander V. KNYAZEV 

Department of Analytical and Medicinal Chemistry, Faculty of Chemistry, Lobachevsky University, Nizhny Novgorod, Russia

Received: 02.02.2021 • Accepted/Published Online: 19.06.2021 • Final Version: 19.10.2021

Abstract: The paper describes methods for the preparation of compounds with an apatite structure containing only iodine atoms in the “halogen” position. The crystal structure of the compounds was refined by the Rietveld method. The resulting apatites have a structure with a space group $P6_3/m$ and have the following unit cell parameters: $\text{Ba}^{4f}_{1.78(2)}\text{Ba}^{6h}_{2.75(2)}(\text{PO}_4)_3\text{I}_{0.04(2)}$ ($a = 10.18609(34) \text{ \AA}$, $c = 7.71113(30) \text{ \AA}$, $V = 692.889(54) \text{ \AA}^3$, $R = 5.448 \%$), $\text{Pb}^{4f}_{1.82(2)}\text{Pb}^{6h}_{2.75(2)}(\text{PO}_4)_3\text{I}_{0.13(2)}$ ($a = 9.87882(18) \text{ \AA}$, $c = 7.43222(16) \text{ \AA}$, $V = 628.144(26) \text{ \AA}^3$, $R = 8.533 \%$), $\text{Pb}^{4f}_{1.90(2)}\text{Pb}^{6h}_{2.68(2)}(\text{PO}_4)_3\text{I}_{0.16(2)}$ ($a = 9.87058(48) \text{ \AA}$, $c = 7.41255(46) \text{ \AA}$, $V = 625.437(72) \text{ \AA}^3$, $R = 5.433 \%$). The study of the crystal structure showed a relatively low efficiency of the binding of iodine in the apatite matrix.

Key words: Iodine, apatite, synthesis, crystal structure, Rietveld refinement

1. Introduction

Currently, 37 isotopes of iodine are known. Among them, the greatest attention is paid to iodine-129: it is one of the seven long-lived fission products of uranium and plutonium and in significant quantities entered the atmosphere as a result of nuclear tests in the 1950s and 1960s [1]. At the same time, it also poses a danger to humans, as a more rapidly decaying iodine-131, since, due to its nature, it can accumulate in the body.

To bind various isotopes of iodine, including iodine-129, many approaches have been proposed [2, 3]:

- mercurex-process, implying receipt of its mercury compounds,
- iodox-process, allowing to fix iodine in the form of solid precipitate HI_3O_8 ,
- use of sorbents based on titanium oxide, copper, silver.

In a number of works [4–6], it was proposed to use a matrix with the structure of the mineral apatite for binding isotopes of iodine, in particular, long-lived iodine-129 ($T_{1/2} = 1.57(4) \cdot 10^7$ years).

The structural type of apatite is known for its high isomorphous capacity, due to which it can undergo substitutions in the structure by almost all atoms of the periodic table and within wide quantitative limits [7, 8]. It should also be noted that, unlike the structural types traditionally used as the basis of matrices for binding radionuclides (garnet, perovskite, hollandite, monazite, etc. [9, 10]), apatites are able to bind not only cations but also anions; therefore, the attention directed at them in the context of radioactive iodine binding is quite justified.

The general formula of apatites can be described as follows: $\text{M}^{4f}_2\text{M}^{6h}_3(\text{AO}_4)_3\text{L}$, where M stands for cations of different oxidation states, located in two crystallographically different positions of the structure, A refers to the most often atoms prone to the formation of tetrahedral coordination polyhedra (for example, P, V, Si, S), and L is for halogens or OH-groups, as well as O^{2-} , CO_3^{2-} and other ions. The content of cations in the structure is rather high; therefore, geoceramics, including apatites, are studied to bind strontium-90 [11, 12]. Taking into account the crystal-chemical similarity of apatite to the mineral part of the native bone of mammals, similar processes can be observed in the human body: at this limit of strontium accumulation in bone tissue, thermodynamic modeling is possible [13].

Attempts to theoretically predict the possibility of binding iodine by the apatite structure were undertaken earlier [14], but a more detailed result was obtained in [15], where, based on machine learning, density functional theory, DFT (density functional theory), and experimental data 18 new thermodynamically stable compounds with the apatite structure containing iodine anions were predicted. Since the attention to the issue of the efficiency of the binding of iodine by the apatite matrix does not decrease [16, 17], an attempt is made in this work to partially reproduce and expand the results of theoretical modeling.

* Correspondence: bulanoven@chem.unn.ru

2. Materials and methods

2.1. Synthesis

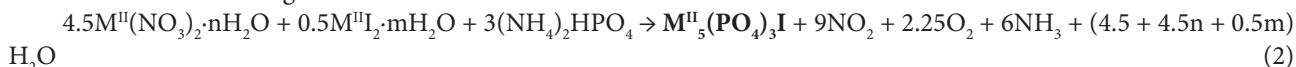
To obtain iodine-apatites, two approaches were considered, namely wet and solid-state approaches.

In the solution method of synthesis, 0.5 M solutions of nitrate of the corresponding divalent cation, ammonium hydrogen phosphate, and a solution containing a 2-fold excess of potassium iodide were used. The general scheme of the reaction can be represented as follows:



The resulting precipitates were kept in the mother liquor for a day, then centrifuged with rinsing with bidistilled hot water and dried in air.

Solid-phase synthesis implied the preparation of a stoichiometric mixture of ammonium hydrogen phosphate, as well as nitrate and iodide of a divalent cation. The reaction mixture was calcined sequentially at temperatures of 300°C, 500°C, and 800°C. The calcination time was 4 h at each stage with the dispersion of the mixture in an agate mortar during the transition to each next stage.



Both approaches are simpler in terms of hardware design than the microwave synthesis proposed in [18], the mechanochemically activated method in [19], or the synthesis using electro-pulse plasma sintering in [4]. The particular amounts of used compounds are given in Table 1.

We used reagents manufactured by the Vekton company of analytical grade and chemically pure grade, except for lead (II) iodide, which was synthesized by the solution method by the reaction of saturated solutions of lead nitrate and potassium iodide and characterized by X-ray diffraction.

2.2. Research methods

The phase individuality of the obtained compounds was monitored using a Shimadzu XRD 6000 powder diffractometer. Powder X-ray diffraction patterns were taken in the 2θ angle range of 10–60 °, on an X-ray tube with a copper cathode (λ (CuK α) = 1.5406 Å) at a voltage of 30 kV and a current 30mA.

Table 1. Amounts of compounds used in two synthetic approaches.

Wet synthesis				
Target compound composition	V (M(NO ₃) ₂ ·4H ₂ O, 0.5 M) (ml)	V ((NH ₄) ₂ HPO ₄ , 0.5 M) (ml)	V (KI, 0.5 M) (ml)	m (apatite) (g)
Ca ₅ (PO ₄) ₃ I	42.3	25.4	16.9	not apatite
Sr ₅ (PO ₄) ₃ I	47.3	28.4	18.9	not apatite
Ba ₅ (PO ₄) ₃ I	38.3	23.0	15.3	not apatite
Cd ₅ (PO ₄) ₃ I	32.4	19.5	13.0	not apatite
Pb ₅ (PO ₄) ₃ I	30.2	18.1	12.1	3.5974
Solid-state synthesis				
Target compound composition	m (M(NO ₃) ₂ ·4H ₂ O) (g)	m ((NH ₄) ₂ HPO ₄) (g)	m (MI ₂ ·nH ₂ O) (g)	m (apatite) (g)
Ca ₅ (PO ₄) ₃ I	5.0000	1.6776	1.2445	not apatite
Sr ₅ (PO ₄) ₃ I	5.0000	1.8720	1.6133	not apatite
Ba ₅ (PO ₄) ₃ I	5.0000	1.5159	1.6345	4.1191 ¹
Cd ₅ (PO ₄) ₃ I	5.0000	1.2843	1.1872	not apatite
Pb ₅ (PO ₄) ₃ I	5.0000	1.1961	1.3919	3.6936 ²

¹with barium phosphate (comments in text).

²after losing of the greater part of PbI₂ (comments in text).

Chemical purity and composition of the obtained sample were studied with Shimadzu XRF-1800 spectrometer using fundamental parameters (FP) method with using standard example. BaK_{α} , CaK_{α} , PbK_{α} , IK_{α} , PK_{α} lines intensities were measured three times at 40 kV, 50 mA on Rh anode with FPC detector for P, and SC detector for Ca, Ba, Pb, I (Table 1). Investigation of the chemical composition of the samples was also performed on method energy dispersive X-ray microanalysis (EDXMA) with Oxford Instruments X-MaxN 20 detector.

To refine the crystal structure, the method of full-profile X-ray analysis (the Rietveld method) was used [20]. The X-ray diffraction patterns were taken on the same diffractometer in the 2θ angle range of 10–120°, the X-ray tube voltage of 40 kV and the current strength of 40 mA, the exposure at a point was 11 s. The structures of known apatites with large halogens $Sr_5(PO_4)_3Br$ [21], $Cd_5(VO_4)_3I$ [22], and $Pb_5(VO_4)_3I$ [19] were considered as primary models. The pseudo-Voigt function (PV_TCHZ) was used to describe the peak profile. The crystal structure was refined using the Topas 3.0 software package.

To estimate the particle size, we used both the data on the refinement of the crystal structure of the Topas 3.0 program and calculations using the Scherrer formula:

$$d = \frac{k\lambda}{\beta \cos \theta} \quad (3)$$

where d is the average crystal size, K is the dimensionless particle shape factor (Scherrer's constant, for spherical particles is considered equal to 0.9), λ is the wavelength of X-ray radiation, β is the width of the reflection at half height, θ is the diffraction angle [23].

Microscopic studies by high-resolution transmission electron microscopy were performed on a JOEL JEM2100F transmission microscope at a voltage of 200 kV, and by atomic scanning microscopy on an AURIGA CrossBeam Workstation (Carl Zeiss).

3. Results

In this work, an attempt was made to obtain iodide-trisphosphates of a number of divalent cations (Ca, Sr, Ba, Cd, Pb) with an apatite structure.

X-ray phase analysis of precipitates obtained in the course of solution synthesis, as well as polycrystalline samples obtained by the solid-phase method, showed that, in the overwhelming majority of cases, orthophosphates of the corresponding divalent cations were obtained. The exceptions were solution synthesis with lead (hereinafter PbPI (w)) and solid-phase syntheses with barium and lead (BaPI and PbPI (ss), respectively): their diffraction patterns were similar to the X-ray diffraction patterns of compounds with apatite structure presented in the inorganic crystal structure database (ICSD).

X-ray fluorescence analysis showed (Table 2) that the amount of bound iodine in the resulting precipitates is significantly less than expected from the theoretical stoichiometry of the compounds (especially in the case of barium compound).

A full-profile X-ray analysis of the obtained compounds showed that their crystal structure corresponds to the type of apatite with the space group $P6_3/m$ of the hexagonal system. In addition, the quantitative phase analysis of the obtained

Table 2. X-ray fluorescence analysis data for synthesized¹ compounds.

Target compound composition	BaO (wt%)			P ₂ O ₅ (wt%)			BaI ₂ (wt%)		
	calc	found ²	found ³	calc	found ²	found ³	calc	found ²	found ³
Ba ₅ (PO ₄) ₃ I	62.82	75.76	75.74	19.38	23.38	23.42	17.80	0.86	0.84
	PbO (wt%)			P ₂ O ₅ (wt%)			PbI ₂ (wt%)		
	calc	found ²	found ³	calc	found ²	found ³	calc	found ²	found ³
Pb ₅ (PO ₄) ₃ I	69.37			14.71			15.92		
solid-state		80.56	80.54		17.08	17.08		2.36	2.38
wet		80.02	80.02		16.96	17.00		3.02	2.98

¹Standard uncertainties u are $u(\text{wt}) = 0.02\%$.

²Shimadzu XRF-1800.

³JEOL JSM-IT300LV with Oxford Instruments X-MaxN 20 detector.

samples showed that the BaPI sample contains a significant impurity of barium phosphate, the structure of which was taken from [24]. The phase analysis of the lead-containing samples showed the absence of any secondary phases in the final product (Figure 1a–1c, Table 3). In the case of PbPI-ss, it can be explained by the absorption of most of the melt of lead iodide by the material of the alundum crucible ($T_m(\text{PbI}_2) = 412^\circ\text{C}$).

As you can see from the Table 4, all three obtained apatites are characterized by a high defectiveness of the positions occupied by halogen, which indicates the low efficiency of the structural type of apatite in relation to the binding of iodine ions, despite the rather optimistic forecast in [15]. In this case, iodine ions are located in the crystallographic position $2b(0; 0; 0)$, which is located on one side in the hexahedral tunnel of the structure formed by three-cap trigonal prisms $M^{\text{II}}\text{O}_9$ (Figure 2a), on the other hand, between quasi-layers formed by phosphate tetrahedra and polyhedra $M^{\text{VI}}\text{O}_6\text{I}_2$ (Figure 2b), which is typical for halogens larger than fluorine in the apatite structure [25–27].

The significantly broader diffraction maxima of PbPI (w) as compared to other obtained apatites indicate the nanoscale of the sample particles. According to calculations using the Scherrer formula and when refining the structure using the Rietveld method, the particle size is 19.6 and 27.6 nm, respectively. The particle size was also confirmed by a direct method - atomic scanning microscopy (Figure 3).

The abnormal values of the crystal structure distortion index of the obtained apatites are presumably related to the particle size. In a number of works by T. White and colleagues [7, 28], the angle φ is the angle of rotation of the bases of three-point trigonal prisms $M^{\text{II}}\text{O}_9$ relative to each other - is considered as such an indicator (Figure 4). As you can see from the Table 5, the value of this index for the PbPI (w) sample is as close to 0° as possible, while BaPI and PbPI (ss) have the values of the angle φ typical for apatites with large divalent cations [7].

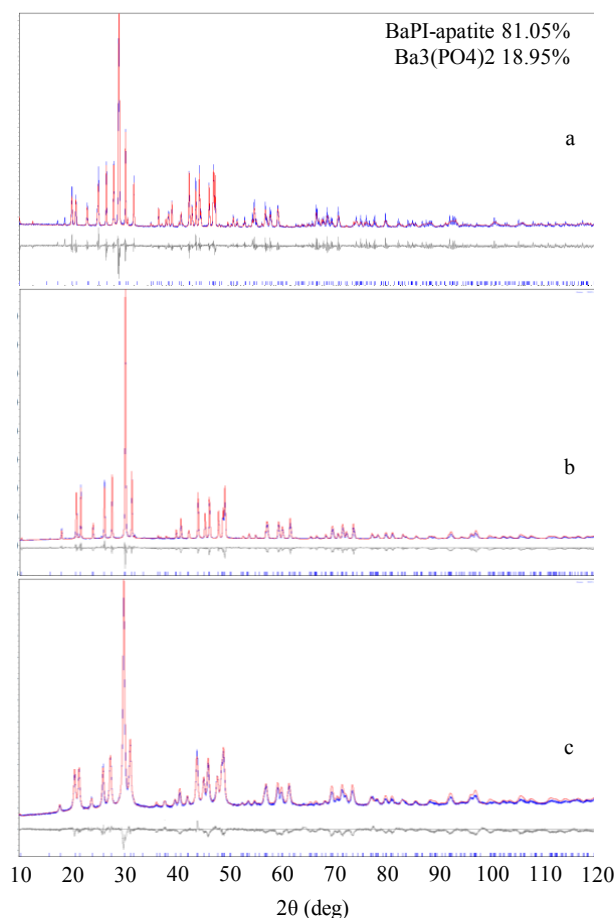


Figure 1. Experimental (blue), calculated (red), difference (gray), and stroke X-ray diffraction patterns of the obtained compounds: BaPI - a, PbPI (ss) - b, PbPI (w) - c.

Table 3. Parameters and results of full-profile X-ray analysis of the crystal structures of the synthesized iodine-apatites.

	BaPI	PbPI(ss)	PbPI(w)
Space group	$P6_3/m$		
a (Å)	10.18609(34)	9.87882(18)	9.87058(48)
c (Å)	7.71113(30)	7.43222(16)	7.41255(46)
V (Å³)	692.889(54)	628.144(26)	625.437(72)
M (g·mol⁻¹)	910.7(96)	1246.7(60)	1255.0(81)
Crystal size (nm)	331(64)	203.1(85)	27.58(63)
Density (g·cm⁻³)	4.365(23)	6.591(16)	6.664(21)
Coefficients of pseudo-Voigt function			
U	1.014(55)	-0.205(10)	0.133(38)
V	-0.7411(25)	0.1424(72)	0.008(32)
Q	0.1300(14)	-0.0229(12)	-0.0187(66)
Z	0	0	0
X	0.000(12)	0.0542(56)	0.000(17)
Y	0	0	0
Scale factor	0.00013737(86)	0.0003990(11)	0.00013517(44)
R-Bragg (%)	5.448	8.533	5.433

Table 4. Atomic coordinates and occupancies of positions of synthesized iodine apatites.

Atom	Wyckoff position	x	y	z	Occ
BaPI					
Ba1	4f	1/3	2/3	-0.0001(13)	0.8871(43)
Ba2	6h	0.24113(50)	-0.01859(52)	1/4	0.9152(29)
P	6h	0.3974(19)	0.3632(21)	1/4	1
O1	6h	0.3446(40)	0.4772(35)	1/4	1
O2	6h	0.5808(38)	0.4778(36)	1/4	1
O3	12i	0.3579(19)	0.2752(20)	0.0698(25)	1
I	2b	0	0	0	0.040(24)
PbPI(ss)					
Pb1	4f	1/3	2/3	0.0020(14)	0.9090(22)
Pb2	6h	0.24605(35)	-0.00024(57)	1/4	0.9152(16)
P	6h	0.3911(12)	0.3603(15)	1/4	1
O1	6h	0.3446(28)	0.5118(24)	1/4	1
O2	6h	0.5792(26)	0.4796(28)	1/4	1
O3	12i	0.3508(15)	0.2670(17)	0.0716(18)	1
I	2b	0	0	0	0.127(13)
PbPI(w)					
Pb1	4f	1/3	2/3	0.01250(74)	0.9498(30)
Pb2	6h	0.24646(37)	-0.00620(59)	1/4	0.8940(21)
P	6h	0.3859(16)	0.3412(21)	1/4	1
O1	6h	0.3942(38)	0.4796(26)	1/4	1
O2	6h	0.6095(44)	0.4803(33)	1/4	1
O3	12i	0.3337(17)	0.2403(18)	0.0672(24)	1
I	2b	0	0	0	0.163(18)

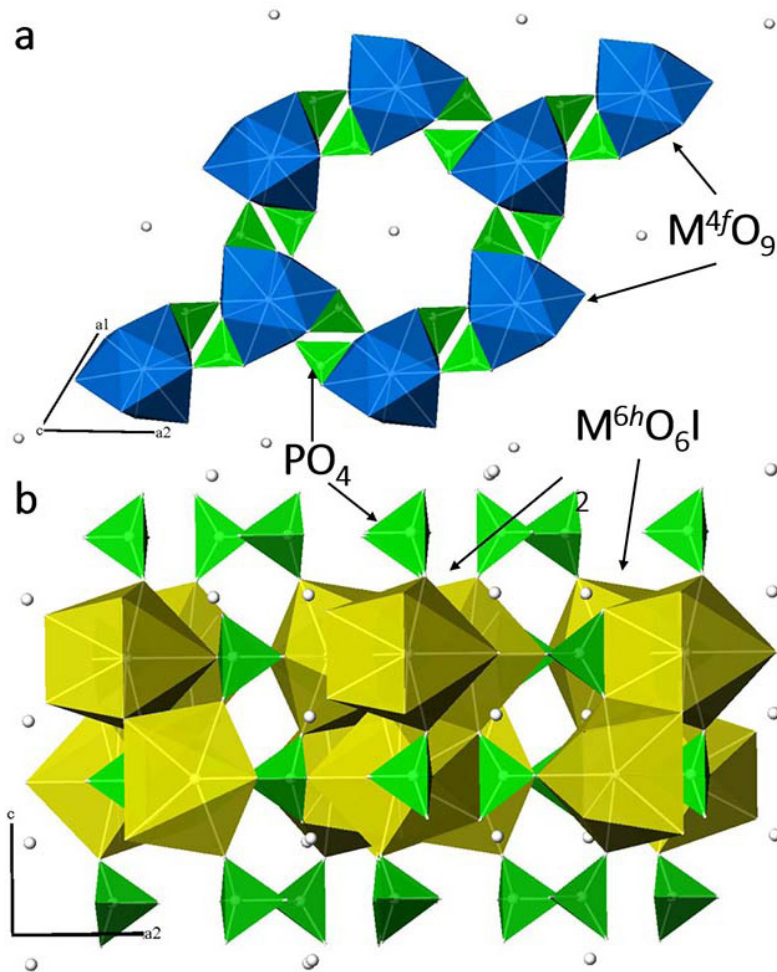


Figure 2. Schematic representation of the crystal structure of the obtained iodine apatites. All positions of iodine atoms are indicated by white spheres in the figure.

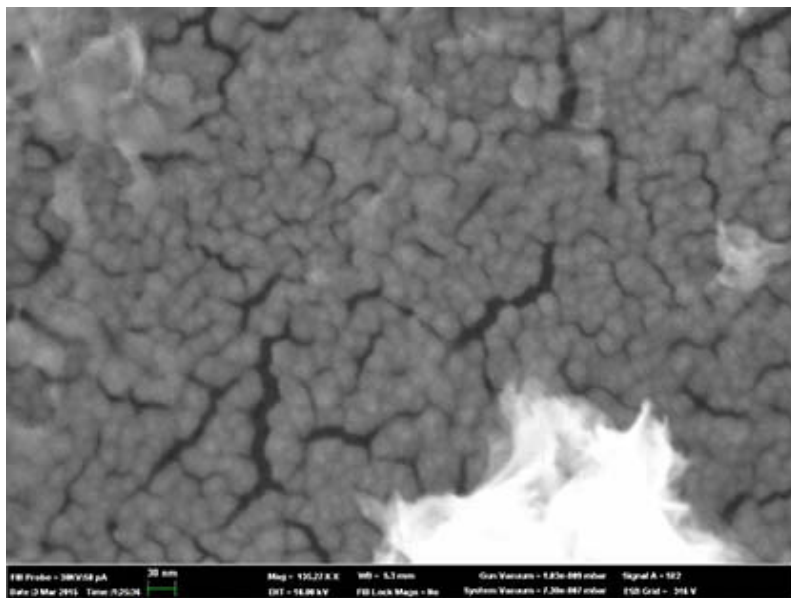


Figure 3. AFM image of PbPI(w) nanospheres. The average particle size is 25–30 nm.

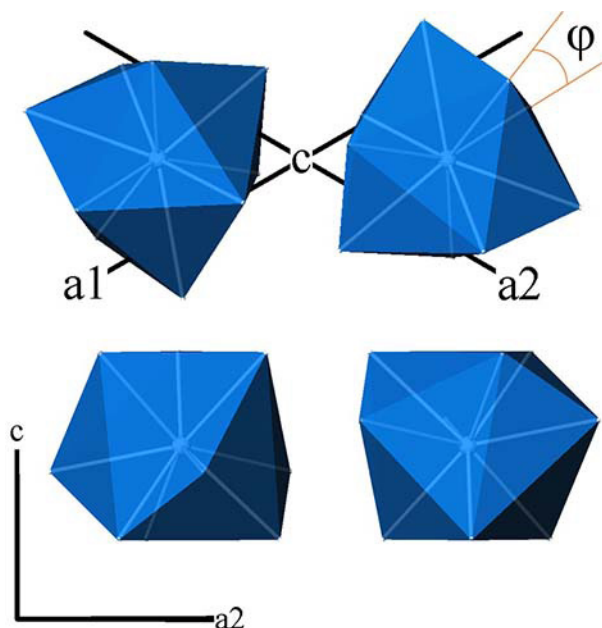


Figure 4. General view of M^fO_9 polyhedra in projections onto different crystallographic planes and the “twist angle” φ , which serves as a criterion for the distortion of the crystal structure of apatites.

Table 5. Parameters of the coordination polyhedrons of cations in the crystal structure of the synthesized iodine-apatites.

	BaPI	PbPI(ss)	PbPI(w)
$M^f-O1 \times 3$	2.771(30)	2.433(20)	2.651(30)
$M^f-O2 \times 3$	2.817(33)	2.755(25)	2.824(28)
$M^f-O3 \times 3$	2.944(21)	2.902(15)	2.996(17)
φ (deg)	18.8	18.3	2.1
$M^{6h}-O2$	2.487(31)	2.376(22)	2.335(28)
$M^{6h}-O3 \times 2$	2.618(19)	2.571(14)	2.494(18)
$M^{6h}-O1$	2.929(32)	3.087(21)	2.531(18)
$M^{6h}-O3 \times 2$	2.956(19)	2.658(16)	3.168(27)
$M^{6h}-I \times 2$	3.190(18)	3.060(26)	3.083(12)
P-O1	1.504(45)	1.628(23)	1.327(37)
P-O3 $\times 2$	1.593(21)	1.549(15)	1.607(20)
P-O2	1.634(31)	1.772(34)	1.930(37)

It should also be noted that, according to high-resolution transmission electron microscopy data, during the synthesis of PbPI (ss), whiskers were formed in the sample - one-dimensional dislocation-free crystals 50–100 nm long and 5–10 nm wide (Figure 5a). Figures 5b and 5c also show the crystal structures of agglomerated whiskers. Such whiskers can play the role of a native reinforcing agent when creating a ceramic material based on this compound.

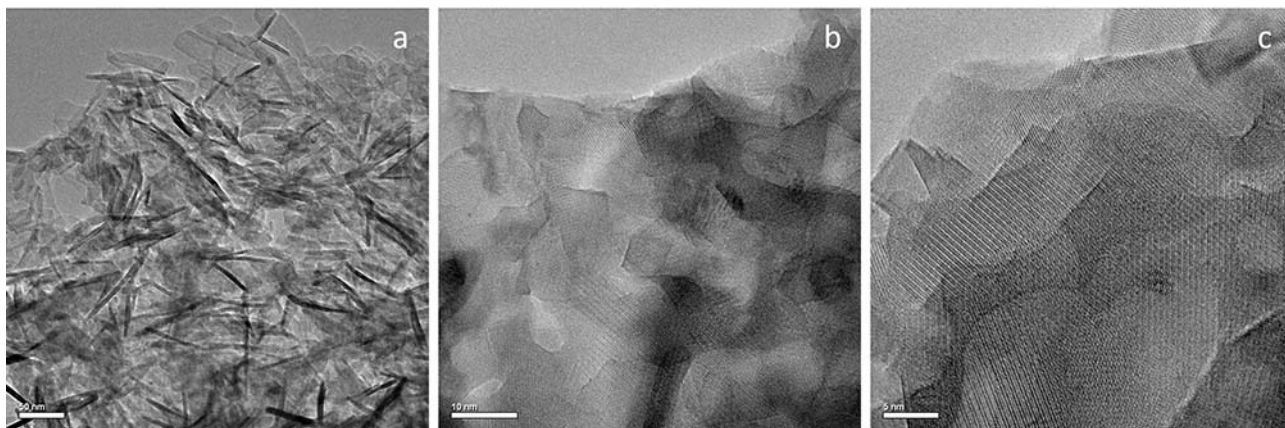


Figure 5. HRTEM image of the microstructure of a PbPI (ss) sample: a - general view of whiskers, b, c - atomic structure of whiskers.

4. Conclusion

Despite the theoretical prediction of the possibility of obtaining various iodine-apatites, in particular, only one iodide triphosphates, solution and solid-phase methods were able to obtain two individual compounds, the compositions of which can be described by the following formulas $\text{Ba}^{4f}_{1.78(2)}\text{Ba}^{6h}_{2.75(2)}(\text{PO}_4)_3\text{I}_{0.04(2)}$, $\text{Pb}^{4f}_{1.82(2)}\text{Pb}^{6h}_{2.75(2)}(\text{PO}_4)_3\text{I}_{0.13(2)}$ (ss), $\text{Pb}^{4f}_{1.90(2)}\text{Pb}^{6h}_{2.68(2)}(\text{PO}_4)_3\text{I}_{0.16(2)}$ (w), and pentalead iodide triphosphate was not considered as possible. Despite the low iodine content in the obtained phases, such nonstoichiometric compounds, nevertheless, proved to be quite stable, but only for the largest cations of the studied series, barium and lead. This can be explained by the fact that iodine cations are located between the layers of the structure formed by phosphate tetrahedra, while the interlayer distance is precisely determined by the size of the cation at the $4f$ crystallographic position. In addition, phosphate phases with completely vacant halogen positions (for example, $\text{Pb}_9(\text{PO})_6\text{I}$ [29]) are known, which have an apatite structure despite the absence of a halogen. This can be attributed to the stability of the obtained phases, which have a largely similar composition and structure and differ only in the presence of a small amount of halogen and an additional amount of cation necessary to maintain electroneutrality.

An analysis of the crystal structure of the obtained compounds showed that these phases bind about 80% less iodine ions from the theoretically expected amount, which cannot speak in their favor as a promising basis for creating a matrix for binding radioactive iodine. However, it should be noted that, during the solid-phase synthesis of PbPI-apatite, nanowhiskers are formed directly in the polycrystalline sample, which can have a favorable effect on the strength characteristics of ceramic materials based on it. Moreover, phosphates with the apatite structure are characterized by higher melting points and polymorphic transformations [30], which makes them more preferable as a chemical base of ceramics for binding radioactive isotopes of iodine.

Acknowledgements

We acknowledge the Ministry of Science and Higher Education agreement No. 075-15-2020-808. We are also grateful to the staff of the School of Materials Science and Engineering of Nanyang Technological University (Singapore) and prof. S.K. Filatov from St.Petersburg State University (Russia) for conducting microscopic studies and assistance in the interpretation of the structural data.

References

1. Edwards RR. Iodine-129: Its occurrence in nature and its utility as a tracer. *Science* 1962; 137 (3533): 851-853. doi: 10.1126/science.137.3533.851
2. Moore RC, Pearce CI, Morad JW, Chatterjee S, Levitskaia TG et al. Iodine immobilization by materials through sorption and redox-driven processes: A literature review. *Science of the Total Environment* 2020; 716: 132820. doi: 10.1016/j.scitotenv.2019.06.166
3. Riley BJ, Vienna JD, Strachan DM, McCloy JS, Jerden JL. Materials and processes for the effective capture and immobilization of radioiodine: A review. *Journal of Nuclear Materials* 2016; 470: 307-326. doi: 10.1016/j.jnucmat.2015.11.038
4. Le Gallet S, Campayo L, Courtois E, Hoffmann S, Grin Y et al. Spark plasma sintering of iodine-bearing apatite. *Journal of Nuclear Materials* 2010; 400 (3): 251-256. doi: 10.1016/j.jnucmat.2010.03.011

5. Campayo L, Le Gallet S, Perret D, Courtois E, Cau Dit Coumes C et al. Relevance of the choice of spark plasma sintering parameters in obtaining a suitable microstructure for iodine-bearing apatite designed for the conditioning of I-129. *Journal of Nuclear Materials* 2015; 457: 63-71. doi: 10.1016/j.jnucmat.2014.10.026
6. Coulon A, Laurencin D, Grandjean A, Le Gallet S, Minier L et al. Key parameters for spark plasma sintering of wet-precipitated iodate-substituted hydroxyapatite. *Journal of the European Ceramic Society* 2016; 36 (8): 2009-2016. doi: 10.1016/j.jeurceramsoc.2016.02.041
7. White T. Apatite - An Adaptive Framework Structure. *Reviews in Mineralogy and Geochemistry* 2005; 57 (1): 307-401. doi: 10.2138/rmg.2005.57.10
8. Tite T, Popa AC, Balescu LM et al. Cationic substitutions in hydroxyapatite: Current status of the derived biofunctional effects and their in vitro interrogation methods. *Materials (Basel)* 2018; 11 (11): 1-62. doi: 10.3390/ma11112081
9. Potanina E, Golovkina L, Orlova A, Nokhrin A, Boldin M et al. Lanthanide (Nd, Gd) compounds with garnet and monazite structures. Powders synthesis by "wet" chemistry to sintering ceramics by Spark Plasma Sintering. *Journal of Nuclear Materials* 2016; 473: 93-98. doi: 10.1016/j.jnucmat.2016.02.014
10. Orlova AI, Ojovan MI. Ceramic mineral waste-forms for nuclear waste immobilization. *Materials (Basel)* 2019; 12 (16): 2638. doi: 10.3390/ma12162638
11. Bogdanov RV, Kuznetsov RA. Aluminosilicophosphate geoceramics as matrices for the immobilization of partitioned 90Sr and 137Cs wastes. *Radiochemistry* 2006; 48 (2): 204-211. doi: 10.1134/S1066362206020202
12. Kuznetsov RA, Platonova NV, Bogdanov RV. A polyphase geoceramic matrix for joint immobilization of the strontium-caesium and rare earth fractions of high-level waste. *Radiochemistry* 2015; 57 (2): 200-206. doi: 10.1134/S1066362215020137
13. Bulanov EN, Knyazev AV, Lelet MI. Thermodynamic Modeling of Integration of Strontium into Bone Tissue Hydroxyapatite. *Applied Solid State Chemistry* 2017; 1 (1): 42-47. doi: 10.18572/2619-0141-2017-1-1-42-47
14. Wang J. Incorporation of iodine into apatite structure: A crystal chemistry approach using Artificial Neural Network. *Frontiers in Earth Science* 2015; 3 (June): 1-11. doi: 10.3389/feart.2015.00020
15. Hartnett TQ, Ayyasamy MV, Balachandran P V. Prediction of new iodine-containing apatites using machine learning and density functional theory. *MRS Communications* 2019; 9 (3): 882-890. doi: 10.1557/mrc.2019.103
16. Venkatesan S, Hassan Mul, Ryu HJ. Adsorption and immobilization of radioactive ionic-corrosion-products using magnetic hydroxyapatite and cold-sintering for nuclear waste management applications. *Journal of Nuclear Materials* 2019; 514: 40-49. doi: 10.1016/j.jnucmat.2018.11.026
17. Zhang Z, Ebert WL, Yao T, Lian J, Valsaraj KT et al. Chemical Durability and Dissolution Kinetics of Iodoapatite in Aqueous Solutions. *ACS Earth and Space Chemistry* 2019; 3 (3): 452-462. doi: 10.1021/acsearthspacechem.8b00162
18. Stennett MC, Pinnock IJ, Hyatt NC. Rapid synthesis of $Pb_5(VO_4)_3I$ for the immobilisation of iodine radioisotopes, by microwave dielectric heating. *Journal of Nuclear Materials* 2011; 414 (3): 352-359. doi: 10.1016/j.jnucmat.2011.04.041
19. Suetsugu Y. Synthesis of lead vanadate iodoapatite utilizing dry mechanochemical process. *Journal of Nuclear Materials* 2014; 454 (1-3): 223-229. doi: 10.1016/j.jnucmat.2014.07.073
20. Rietveld HM. The Rietveld method. *Physica Scripta* 2014; 89 (9). doi: 10.1088/0031-8949/89/9/098002
21. Alberius-Henning P, Mattsson C, Lidin S. Crystal structure of pentastronium tris (phosphate) bromide, $Sr_5(PO_4)_3Br$ and of pentabarium tris(phosphate) bromide $Ba_5(PO_4)_3Br$, two bromoapatites. *Zeitschrift für Kristallographie - New Crystal Structures* 2000; 215 (3): 345-346. doi: 10.1515/ncrs-2000-0319
22. Sudarsanan K, Young RA, Wilson AJC. The structures of some cadmium 'apatites' $Cd_5(MO_4)_3X$. I. Determination of the structures of $Cd_5(VO_4)_3I$, $Cd_5(PO_4)_3Br$, $Cd_5(AsO_4)_3Br$ and $Cd_5(VO_4)_3Br$. *Acta Crystallographica Section B: Structural Science* 1977; 33 (10): 3136-3142. doi: 10.1107/s0567740877010413
23. Patterson AL. The scherrer formula for X-ray particle size determination. *Physical Review* 1939; 56 (10): 978-982. doi: 10.1103/PhysRev.56.978
24. Sugiyama K, Tokonami M. The crystal structure refinements of the strontium and barium orthophosphates. *Mineralogical Journal* 1990; 141-146.
25. Hata M, Marumo F, Iwai S, Aoki H. Structure of barium chlorapatite. *Acta Crystallographica Section B: Structural Science* 1979; 35 (10): 2382-2384. doi: 10.1107/s0567740879009377
26. Elliott JC, Dykes E, Mackie PE. Structure of bromapatite and the radius of the bromide ion. *Acta Crystallographica Section B: Structural Science* 1981; 37 (2): 435-438. doi: 10.1107/s0567740881003208
27. Henning PA, Lidin S, Petříček V. Iodo-oxyapatite, the first example from a new class of modulated apatites. *Acta Crystallographica Section B: Structural Science* 1999; 55 (2): 165-169. doi: 10.1107/s0108768198012312

28. Lim SC, Baikie T, Pramana SS, Smith R, White TJ. Apatite metaprism twist angle (φ) as a tool for crystallochemical diagnosis. *Journal of Solid State Chemistry* 2011; 184 (11): 2978-2985. doi: 10.1016/j.jssc.2011.08.031
29. Hata M, Marumo F, Iwai SI. Structure of a Lead Apatite $Pb_9(PO_4)_6$. *Acta Crystallographica B* 1980; 36: 2128-2130. doi: 10.1107/S0567740880008096
30. Chernorukov NG, Knyazev AV, Bulanov EN. Phase transitions and thermal expansion of apatite-structured compounds. *Inorganic Materials* 2011; 47 (2): 172-177. doi: 10.1134/S002016851101002X